two quanta of the bend or stretch. With these assignments, it was impossible to reproduce all of the peak intensities within the uncertainties of the experiment. Thus, the assignment of the vibrational origin is unambiguously confirmed.

C. Comparison with Previous Experiments and Theory. Table IV compares the present result with other experimental and theoretical molecular geometries for NO_2^- . Ab initio self-consistent-field (SCF) calculations for NO_2^- give bond lengths in the range 1.22–1.26 Å and bond angles of 117–118°. These values agree well with the present results. The geometric constants of NO_2^- in crystalline environments differ from our determination for gas-phase NO_2^- by only a few percent. This result is consistent with the ab initio results of Goddard and Klein, ¹⁶ who calculated the structure of NO_2^- interacting with one or two sodium ions and found only modest changes in the NO_2^- geometry. Ozone, which is isoelectronic with NO_2^- , has a bond length of 1.278 Å and a bond angle of 116.8°, ⁵³ quite close to the geometry found for here for NO_2^- .

Our conclusions regarding the anion geometry suggest a reinterpretation of the results of Woo et al.⁵ They modeled photodetachment threshold data for NO₂⁻ at photon energies up to 2.8 eV using a Franck-Condon analysis, in which the Franck-Condon intensities were derived from the increase in the photodetachment cross section at the threshold for each transition. The magnitude and behavior of the photodetachment cross section beyond the threshold region were fixed by a fit to their data in the ultraviolet, 3.5-4.8 eV. Woo et al. found two possible fits, r'' = 1.25 Å, α'' = 116° and r'' = 1.15 Å, α'' = 119.5°, corresponding to opposite directions of the displacement in the ν_1 symmetric stretch normal coordinate. The latter geometry gave a better least-squares fit to the threshold data (by a factor of 10 in the sum of squared residuals of Franck-Condon factors), and it was chosen by Woo et al. primarily on that basis. Our observations provide intensities for individual transitions directly, which should be more sensitive to small difference in Franck-Condon intensities than threshold measurements, and we also observe higher vibrational transitions. We find no direct experimental basis for determing the direction

of the geometry displacements. We believe the molecular orbital considerations and comparisons to ab initio calculations, above, argue convincingly in favor of the configuration with longer bond length and smaller bond angle. In particular, it seems unlikely that the SCF calculations of the bond lengths (Table IV) are in error by 0.07–0.11 Å (6–10%). Therefore, we suggest a reinterpretation of the data of Woo et al. in favor of their alternative NO_2^- geometry (r''=1.25 Å, $\alpha''=116^\circ$), which agrees well with the present work and with theoretical values. A possible source of the discrepancy is photodetachment to electronically excited states of NO_2 at the higher photon energies in the study of Woo et al., which could alter the shape and magnitude of the cross section and therefore the fitting parameters used for the threshold data.

V. Conclusion

We have measured the 351-nm photoelectron spectrum of NO_2^- . The electron affinity of NO_2 is 2.273 \pm 0.005 eV.

The vibrational spectrum of the ground electronic state of NO_2 is observed within 1 eV of its ground vibrational state. There is no evidence of electronic excited states in this region. In contrast to the highly complicated visible spectrum of NO_2 , the vibrational structure in the energy range studied here is completely described by simple overtone and combination progressions in the two totally symmetric vibrational modes of the ground electronic state. Franck-Condon analysis of the vibrational band intensities provides an estimate of the molecular geometry of the anion: $r'' = 1.25 \pm 0.02$ Å and $\alpha'' = 117.5 \pm 2^{\circ}$ for NO_2^{-} , compared to r' = 1.194 Å and $\alpha' = 133.9^{\circ}$ for $NO_2.40^{\circ}$ The large increase in the bond angle upon removal of an electron from NO_2^{-} is responsible for the extended progression observed in the bend vibrational mode. The symmetric stretch progression is also active due to a decrease in the N-O bond length from NO_2^{-} to NO_2 .

Acknowledgment. We thank Dr. Keith Lykke for his expert work on the design and development of the ultraviolet laser system. We are grateful for helpful discussions with Dr. S. V. ONeil, Professor G. Barney Ellison, and Dr. Sean Moran. This research is supported by National Science Foundation Grants CHE 83-16028 and PHY 86-04508.

Registry No. NO₂⁻, 14797-65-0.

Unimolecular Reaction Rate Theory for Highly Flexible Transition States. 2. Conventional Coordinate Formulas for the Various Possible Fragment Combinations. Miscellaneous Topics

Stephen J. Klippenstein and R. A. Marcus*

Arthur Amos Noyes Laboratory of Chemical Physics, California Institute of Technology,[†] Pasadena, California 91125 (Received: January 26, 1988; In Final Form: March 30, 1988)

A method for using conventional coordinates in the implementation of RRKM theory for unimolecular dissociations was described in part 1 of this series, for the case where both fragment molecules are nonlinear. The corresponding formalism for all possible types of fragments, atomic, linear, and nonlinear fragments and their combinations, is presented here. Also discussed analytically is the tendency, in a unimolecular dissociation, for the position of the transition state to move to shorter fragment–fragment separation distances with increasing total energy E. This tendency has marked consequences, including increasing deviation of rate constants from those of phase space theory with increasing E and, in the case of fragment–fragment recombination, a corresponding tendency for high-pressure rate constants to decrease with increasing temperature. Two other topics considered in this paper are the case of two minima in the variational calculation and the role of the repulsive potential energy curves in the unimolecular dissociations under consideration.

I. Introduction

The number of states $N_{EJ}(R)$ for a given excess energy E, total angular momentum quantum number J, and position R along a reaction coordinate enters into the RRKM theory¹ of unimolecular dissociations. With a sufficiently accurate determination of this

quantity and of the density of states ρ_{EJ} of the molecule itself, good agreement between theoretically and experimentally de-

⁽⁵³⁾ Herzberg, G. Molecular Spectra and Molecular Structure. III. Electronic Spectra and Electronic Structure of Polyatomic Molecules; Van Nostrand Reinhold: New York, 1966; p 604.

[†]Contribution No. 7731. Dedicated to the memory of Ed Lee, whose joyous spirit in research will always be remembered.

⁽¹⁾ Robinson, P. J.; Holbrook, K. A. Unimolecular Reactions; Wiley: New York, 1972. Forst, W. Theory of Unimolecular Reactions; Academic: New York, 1973. Weston, R. E.; Schwarz, H. A. Chemical Kinetics; Prentice-Hall: Englewood Cliffs, NJ, 1972. Marcus, R. A. J. Chem. Phys. 1952, 20, 359. Marcus, R. A.; Rice, O. K. J. Phys. Colloid Chem. 1951, 55, 894. Marcus, R. A. J. Chem. Phys. 1965, 43, 2658; 1970, 52, 1018.

termined rate constants k_{EJ} is anticipated, as long as the statistical assumption is valid. For k_{EJ} we have

$$k_{EJ} = N_{EJ}(R^{\dagger})/h\rho_{EJ} \tag{1}$$

where R^{\dagger} is variationally determined. (A correction for nuclear tunneling along the reaction coordinate, a rare circumstance in dissociations into two polyatomic fragments, may be found in ref

One facet of an accurate treatment of $N_{EJ}(R)$ is the manner in which the "transitional" modes are treated. These transitional modes are those modes which undergo a considerable change in character during the transformation from reactants to products. In particular, these modes are typically the bending/hindered rotor and overall rotational modes of the reactant which change to free rotations and to translations of the products. The remaining modes (apart from the reaction coordinate) have been termed the "conserved" modes and are typically vibrations in both the reactant and product configurations.

Recently, Wardlaw and Marcus³ described a method for treating the transitional mode interactions within a classical framework, while retaining a quantum treatment for the conserved modes. The method of ref 3 for determining $N_{EJ}(R)$ was based on the approximate separation of variables into the transitional modes and conserved modes described above, with a transformation of variables to canonically conjugate action-angle variables being used for the transitional modes. That method also implicitly assumed a reaction coordinate defined by the center-of-mass to center-of-mass separation distance of the two fragments. Subsequently, the present authors calculated the effect of using a quantum mechanical treatment of the transitional modes on thermally averaged rate constants.⁴ This calculation was performed via a Feynman path integration of partition function ratios. It indicated, at least for the reaction studied, the $C_2H_6 \rightarrow 2CH_3$ dissociation reaction, that the quantum mechanical correction for the transitional modes was negligible at the temperatures inves-

The present authors have also shown in part 15 how conventional coordinates could be used to implement RRKM theory in a formalism based on the same separation of variables as that of ref 3. The formalism presented in part 1 was for the specific case of two nonlinear fragments. In the present article expressions are given for the determination of N_{EJ} for the various other possible fragment-fragment cases which arise in practice. In section II a brief summary of the derivation of N_{EJ} 's in terms of conventional coordinates is given. In section III the definition of certain quantities needed in the evaluation of $N_{EJ}(R)$ and which are specific to the given fragment type are given. In particular, the detailed formulas pertaining to the cases of an atomic fragment, a linear fragment, and a nonlinear fragment are considered. In section IV a particular phenomenon is discussed in which the position of the transition state tends to move to shorter fragment-fragment separation distance with increasing total energy. Its consequences are also described there. In section V a third topic is considered: the case of two minima in the plot of the number of states versus reaction coordinate curve, in particular the results which we have obtained in a practical case. In section VI the role (or nonrole) of repulsive potential energy curves in the type of dissociation into two fragments that is being considered is discussed, together with the corresponding question in phase space theory⁶ (PST). Concluding remarks follow in section VII.

II. Theory

Conventional coordinates were introduced in part 1 instead of the action-angle coordinates used earlier³ in calculating N_{EJ} . The reaction coordinate R in part 1 was again taken to be the center-of-mass to center-of-mass separation distance between the two fragments. The approximate separation of variables into the conserved modes and the transitional modes, which was the basis of the previous method,³ results in the number of states being given by the convolution

$$N_{EJ}(R) = \int_0^E N_V(E - \epsilon) \rho_J(\epsilon) \, d\epsilon \qquad (2)$$

where $N_{\nu}(E-\epsilon)$ is the number of quantum states for the conserved modes with an energy less than or equal to $E - \epsilon$, and $\rho_J(\epsilon)$ is the density of states for the transitional modes at the given energy ϵ and total angular momentum quantum number J for the given

The evaluation of $\rho_J(\epsilon)$ involves the choice of a coordinate system. The appropriate coordinate system depends upon whether the fragments have zero, two, or three rotational degrees of freedom. However, in all cases the rotation of the line of centers connecting the two centers of masses of the fragments is a two degree of freedom rotation and so may be described by the coordinates θ_{12} and ϕ_{12} defining the spatial orientation of this line of centers. For the other coordinates, the case of two nonlinear polyatomic fragments (i.e., each a three-dimensional rotor) was considered in part 1 and the coordinates chosen were for the absolute orientation in space of fragment i and were the conventional Euler angles.⁷ If fragment i is, instead, linear, and so is a two-dimensional rotor, the appropriate coordinates for this fragment are the angles θ_i and ϕ_i which describe the absolute orientation in space of the axis of this linear species. When fragment i is an atom, no orientational coordinates are needed for it. The coordinates describing the orientation of fragment i are denoted Ω_i and their conjugate momenta by \mathbf{p}_i , regardless of which type of fragment is being referred to.

With the above choice of coordinate system for the appropriate fragment cases $\rho_J(\epsilon)$ is given, as in part 1, by

$$\rho_{J}(\epsilon) = \frac{g_{\rm e}}{\sigma h^{(n_1 + n_2 + 2)}} \int \delta[\epsilon - H(\tau)] \hbar \delta[J\hbar - J_{\rm T}(\tau)] d\tau \quad (3)$$

where τ denotes the orientational coordinates Ω_i , θ_{12} , and ϕ_{12} and their conjugate momenta and $d\tau$ denotes the corresponding phase space volume element. The quantity J_T in eq 3 is the magnitude of the total angular momentum as a function of the coordinates, whereas J in the second delta function in eq 3 is the total angular momentum quantum number. The quantities n_1 and n_2 are the number of rotational degrees of freedom for fragments 1 and 2; g_e is the electronic degeneracy factor. σ is the usual degeneracy factor for the fragment pair, and σ equals $2\sigma_1\sigma_2$ or $\sigma_1\sigma_2$, according as the fragments are or are not identical; σ_i denotes the symmetry number of fragment i. The Hamiltonian H is given by $H = T^0$ + V, where V is the potential energy and T^0 the total kinetic energy for the transitional modes. T^0 in turn is given by the sum of T_{12}^0 , the kinetic energy for the line of centers rotation and the kinetic energies T_1^0 and T_2^0 of the two fragments. The former is given

$$T_{12}{}^{0} = \frac{1}{2I_{di}{}^{\dagger}} \left(p_{\theta_{12}}{}^{2} + \frac{p_{\phi_{12}}{}^{2}}{\sin^{2}\theta_{12}} \right) \tag{4}$$

with I_{di}^{\dagger} being the diatomic moment of inertia for the line of centers, i.e., I_{di}^{\dagger} equals $M_1 M_2 R^2 / (M_1 + M_2)$, where M_1 and M_2 are the masses of fragments 1 and 2, respectively. The kinetic energy T_i^0 is given in section III for each of the separate fragment cases.

⁽²⁾ Marcus, R. A. J. Chem. Phys. 1966, 45, 2138, 2630. Miller, W. H. J. Am. Chem. Soc. 1979, 101, 6810.

⁽³⁾ Wardlaw, D. M.; Marcus, R. A. Chem. Phys. Lett. 1984, 110, 230. Wardlaw, D. M.; Marcus, R. A. J. Chem. Phys. 1985, 83, 3462. Wardlaw, D. M.; Marcus, R. A. J. Phys. Chem. 1986, 90, 5383. Wardlaw, D. M.; Marcus, R. A. Adv. Chem. Phys. 1988, 70, 231.
(4) Klippenstein, S. J.; Marcus, R. A. J. Chem. Phys. 1987, 87, 3410.

⁽⁵⁾ Klippenstein, S. J.; Marcus, R. A. J. Phys. Chem. 1988, 92, 3105

⁽hereinafter referred to as part 1).
(6) Pechukas, P.; Light, J. C. J. Chem. Phys. 1965, 42, 3281. Pechukas, P.; Rankin, R.; Light, J. C. J. Chem. Phys. 1966, 44, 794. Klotz, C. J. Phys. Chem. 1971, 75, 1526. Klotz, C. Z. Naturforsch, A 1972, 27, 553. Chesnavich, W.; Bowers, M. J. Chem. Phys. 1977, 66, 2306.

⁽⁷⁾ Goldstein, H. Classical Mechanics, 2nd ed.; Addison-Wesley: Reading, MA, 1980. The "y convention" given there in Appendix B is used here. There is a typographical error in the last row of the rotation matrix A there, namely, the ψ 's should be replaced by ϕ 's.

Substituting the above expression for $\rho_J(\epsilon)$ into eq 2 and performing the integration over ϵ yields

$$N_{EJ}(R) = \frac{g_{\rm e}\hbar}{\sigma h^{(n_1 + n_2 + 2)}} \int N_{V}[E - H(\tau)] \delta[J\hbar - J_{\rm T}(\tau)] d\tau \qquad (5)$$

Equation 5 provides an expression for N_{EJ} . Next, the dimension of the phase space integral in eq 5 is reduced as in part 1.

First, the angular momentum is fixed along the z direction by introducing a delta function in $J_T - J_{T,}$, multiplying by the range of $J_{T,}$, $(2J+1)\hbar$, and then transforming from the line of centers coordinates and conjugate momenta to the Cartesian components of the orbital angular momentum (l_x, l_y, l_z) and the line of centers coordinate ϕ_{12} . This transformation is specified by⁸

$$l_x = -p_{\theta_{12}} \sin \phi_{12} - p_{\phi_{12}} \cos \phi_{12} \cot \theta_{12}$$

$$l_y = p_{\theta_{12}} \cos \phi_{12} - p_{\phi_{12}} \sin \phi_{12} \cot \theta_{12}, \quad l_z = p_{\phi_{12}}, \quad (6)$$

with the Jacobian of the transformation being given by

$$\begin{aligned} |\partial(\theta_{12}p_{\theta_{12}}p_{\phi_{12}})/\partial(l_xl_yl_z)| &= |\sin^2\theta_{12}/p_{\phi_{12}}| \\ &= |l_z|/[(\cos\phi_{12}l_x + \sin\phi_{12}l_y)^2 + l_z^2] \end{aligned} \tag{7}$$

With these results the expression for $N_{EJ}(R)$ becomes

$$N_{EJ}(R) = \frac{g_{c}(2J+1)\hbar^{2}}{\sigma h^{(n_{1}+n_{2}+2)}} \times \int N_{V}[E-H(\tau')] \frac{\delta[J\hbar - J_{T}(\tau')]\delta[J_{T}(\tau') - J_{T_{z}}(\tau')]|l_{z}|}{(\cos\phi_{12}l_{x} + \sin\phi_{12}l_{y})^{2} + l_{z}^{2}} d\tau'$$
(8)

where τ' now denotes the coordinates Ω_i , \mathbf{p}_i , ϕ_{12} , l_x , l_y , l_z , and $d\tau'$ is the corresponding volume element.

Next, a transformation is made from l_x , l_y , and l_z to J_T , θ , and ϕ , where the θ and ϕ are the polar coordinates of J_T :

$$l_x + k_x = J_T \sin \theta \cos \phi, \quad l_y + k_y = J_T \sin \theta \sin \phi,$$

$$l_z + k_z = J_T \cos \theta$$
 (9)

Here, k_x , k_y , and k_z are the Cartesian components of the sum of the space-fixed rotational angular momenta of the individual fragments \mathbf{j}_i (e.g., $k_x = j_{x_1} + j_{x_2}$), which in turn are specified in section III for each of the fragment types. The Jacobian of the transformation in eq 9 is given by $|\partial(l_x l_y l_z)/\partial(J_T \theta \phi)| = J_T^2 \sin \theta$

Integration in eq 8, using the delta functions, over $J_{\rm T}$ and θ and then over ϕ_{12} and ϕ , after considering the dependence of the resulting integral on the ϕ , ϕ_i , and ϕ_{12} coordinates, yields

$$N_{EJ}(R) = \frac{g_{e}(2J+1)}{\sigma h^{(n_{1}+n_{2})}} \int N_{V}[E - H(\Omega_{i}, \mathbf{p}_{i}, \phi_{12}^{*}, J\hbar, \theta=0)] \times \frac{|J\hbar - k_{z}|J\hbar}{(\cos \phi_{12}^{*}k_{z} + \sin \phi_{12}^{*}k_{y})^{2} + (J\hbar - k_{z})^{2}} \prod_{i=1}^{2} d\Omega_{i} d\mathbf{p}_{i}$$
(10)

The quantity ϕ_{12}^* defines a fixed azimuthal angle for the line of centers orientation and can be set equal to zero (i.e., $\phi_{12} = \phi_{12}^* = 0$), as was shown in part 1.

The integration over the delta functions also results in expressions for the quantities l_x , l_y , and l_z in terms of the coordinates and momenta Ω_i and \mathbf{p}_i (or alternatively the k's). These expressions, in turn, specify the quantities θ_{12} , ϕ_{12} , $\rho_{\theta_{12}}$, and $\rho_{\phi_{12}}$ in terms of the k's, ϕ_{12}^* , and J_T . More specifically, the coordinates for the orientation of the line of centers (θ_{12}, ϕ_{12}) and their conjugate momenta are specified to be

$$\theta_{12} = \cot^{-1}\left(\frac{k_x \cos \phi_{12}^* + k_y \sin \phi_{12}^*}{J_T - k_z}\right), \quad \phi_{12} = \phi_{12}^*$$

$$p_{\theta_{12}} = k_x \sin \phi_{12}^* - k_y \cos \phi_{12}^*, \quad p_{\phi_{12}} = J_T - k_z \quad (11)$$

The expressions given in eq 11 are used in all terms in the final integral involving these quantities, e.g., in $T_{12}^{\ 0}$ and in the ex-

pressions for the determination of the potential energy given in section III.

With these definitions eq 10 for N_{EJ} provides an expression which can be used for all possible fragment types. By combining eq 10 with the definitions of the various fragment-dependent quantities given in section III, we obtained an explicit expression for N_{EJ} for each fragment case. The integral in eq 10 may be evaluated through Monte Carlo importance sampling by introducing the weighting function $\exp(-\beta T_1^{\ 0}) \exp(-\beta T_2^{\ 0})$. The integral over this weighting function, divided by $h^{n_1+n_2}$, is given by the product $Q_1^{\ 0}Q_2^{\ 0}$ of the free-rotation canonical partition functions for each fragment, 1 and 2. The result of the introduction of this weighting function and a transformation of momenta variables to \mathbf{p}_i , defined in section III for each of the different types of fragments, yields N_{EJ} in the form

$$N_{EJ}(R) = \frac{g_{e}(2J+1)J\hbar}{\sigma} Q_{1}{}^{0}Q_{2}{}^{0} \times \left\{ \frac{N_{V}(E-H)(J\hbar-k_{z}) \exp[\beta(T_{1}{}^{0}+T_{2}{}^{0})]}{(\cos\phi_{12}{}^{*}k_{x}+\sin\phi_{12}{}^{*}k_{y})^{2}+(J\hbar-k_{z})^{2}} \right\}$$
(12)

where $\langle f \rangle$ denotes an average with respect to the free-rotation weight function

$$\langle f \rangle = \frac{1}{Q_1^0 Q_2^0 h^{(n_1 + n_2)}} \int f \exp[-\beta (T_1^0 + T_2^0)] \prod_{i=1}^2 d\Omega_i d\mathbf{p}_i' \left| \frac{\partial \mathbf{p}_i}{\partial \mathbf{p}_i'} \right|$$
(13)

In eq 13 $|\partial \mathbf{p}_i/\partial \mathbf{p}_i'|$ is the Jacobian of the transformation to be given in section III. The explicit definitions of the partition functions Q_i^0 and fragment kinetic energies T_i^0 for the specific cases are also given in section III.

The β in eq 12 and 13 equals $1/k_BT$, where T is a sampling temperature and k_B is Boltzmann's constant. In the calculation this T is chosen to ensure that the maximum kinetic energy sampled is about 2-3 times the maximum available energy.

 N_{EJ} may now be straightforwardly evaluated from eq 12 by using, as in part 1, crude sampling over all space for the orientational coordinates and importance sampling⁹ for the momentum coordinates, with $\exp[-\beta(T_1^0 + T_2^0)]$ as the weighting function. In the importance sampling over the momentum coordinates step sizes which gave a roughly 50% acceptance ratio were typically used in the applications in part 1 and ref 10.

III. Properties of Different Fragments

(a) General Formulas. We consider here the calculation of the potential energy $V(\mathbf{r}_{i,j})$, where $\mathbf{r}_{i,j}$ denotes the space-fixed position of atom j in fragment i, in terms of the orientational coordinates Ω_i , θ_{12} , and ϕ_{12} and the reaction coordinate R. The position $\mathbf{r}_{i,j}$ of atom j in fragment i may be written in terms of its position in space relative to the center of mass of fragment i and in terms of the position of the center of mass of fragment i in space. This latter position is determined by the orientation of the line of centers connecting the two fragments and by the center-of-mass to center-of-mass separation distance. In particular, this position may be written as $\mathbf{A}_{12}^{-1}(\theta_{12},\phi_{12})\mathbf{r}_i'$, where \mathbf{r}_{i}

$$\mathbf{A}_{12}^{-1}(\theta_{12},\phi_{12}) = \begin{pmatrix} \cos\theta_{12}\cos\phi_{12} & -\sin\phi_{12} & \sin\theta_{12}\cos\phi_{12} \\ \cos\theta_{12}\sin\phi_{12} & \cos\phi_{12} & \sin\theta_{12}\sin\phi_{12} \\ -\sin\theta_{12} & 0 & \cos\theta_{12} \end{pmatrix}$$
(14)

and \mathbf{r}_i' is the body-fixed position of the center of mass of fragment

$$\mathbf{r}_{1'} = \left(0, 0, \frac{M_2}{M_1 + M_2}R\right), \quad \mathbf{r}_{2'} = \left(0, 0, -\frac{M_1}{M_1 + M_2}R\right)$$
 (15)

⁽⁹⁾ Valleau, J. P.; Whittington, S. G. In Statistical Mechanics; Berne, B. J., Ed.; Plenum: New York, 1977; p 137. Valleau, J. P.; Torrie, G. M. In Statistical Mechanics; Berne, B. J., Ed.; Plenum: New York, 1977; p 169. (10) Klippenstein, S. J.; Khundkar, L. R.; Zewail, A. H.; Marcus, R. A.

J. Chem. Phys., in press.

$$\mathbf{A}_{i}^{-1}(\mathbf{\Omega}_{i}) = \begin{pmatrix} -\sin \psi_{i} \sin \phi_{i} + \cos \theta_{i} \cos \phi_{i} \cos \psi_{i} \\ \sin \psi_{i} \cos \phi_{i} + \cos \theta_{i} \sin \phi_{i} \cos \psi_{i} \\ -\cos \psi_{i} \sin \theta_{i} \end{pmatrix}$$

and the axis of the body in space is defined by θ_{12} and ϕ_{12} . The position of the center of mass as a whole, as seen from eq 15, is chosen to be at the origin.

The position of atom j of fragment i in space relative to the center of mass of fragment i can be written as $\mathbf{A}_i^{-1}(\Omega_i)\mathbf{r}_{i,j}$, where the $\mathbf{r}_{i,j}$ are the body-fixed coordinates which describe the initial position (prior to any rotations) of atom j in fragment i, relative to the center of mass of fragment i. The orientation of the body-fixed axes of fragment i relative to the space-fixed Cartesian axes is defined by the Ω_i coordinates. The specific form of the inverse rotation matrix $\mathbf{A}_i^{-1}(\Omega_i)$ describing this orientation of the body-fixed axes is discussed later for different types of the fragment.

Thus, finally we have

$$\mathbf{r}_{i,j} = \mathbf{A}_i^{-1}(\mathbf{\Omega}_i)\mathbf{r}_{i,j}' + \mathbf{A}_{12}^{-1}(\theta_{12},\phi_{12})\mathbf{r}_i'$$
 (16)

In sections IIIb to IIId the detailed expressions involved in the determination of N_{EJ} for the different types of fragments are given.

(b) Atomic Fragment. When fragment i is an atom rather than a molecule, there are no orientational coordinates or rotational momenta for this fragment and so the quantities T_i^0 , j_{x_i} , j_{y_i} , j_{z_i} , and n_i are all replaced by zero. The matrix A_i^{-1} is replaced by the 3×3 identity matrix. Also, the free-rotation canonical partition function Q_i^0 is replaced by unity and the differentials $d\Omega_i$, $d\mathbf{p}_i$, and $d\mathbf{p}_i'$ do not appear. The body-fixed coordinates for the atomic fragment i, $\mathbf{r}_{i,1}'$, are just the coordinates of the origin (the center of fragment i), i.e., $\mathbf{r}_{i,1}' = (0,0,0)$.

(c) Linear Fragment. When fragment i is linear, the orientational coordinates are chosen to be the spherical polar angles θ_i and ϕ_i . Their conjugate momenta are denoted by \mathbf{p}_{θ_i} and p_{ϕ_i} , respectively. The transformed momenta are given by $\mathbf{p}_i' = (p_{a_i}, p_{b_i})$ with $p_{a_i} = -p_{\phi_i}/\sin\theta_i$ and $p_{b_i} = p_{\theta_i}$. The Jacobian $|\partial \mathbf{p}_i/\partial \mathbf{p}_i'|$ is thus equal to $\sin\theta_i$.

The kinetic energy for fragment i is given in terms of these transformed momenta by

$$T_i^0 = (p_a^2 + p_h^2)/2I_i^{\dagger} \tag{17}$$

where I_i^{\dagger} is the moment of inertia for fragment i in its transition-state structure. For a diatomic fragment we have, for example, $I_i^{\dagger} = m_1 m_2 r_{\rm e}^2(R)/(m_1 + m_2)$, where m_1 and m_2 are the masses of the two atoms in the diatomic fragment and $r_{\rm e}(R)$ is the equilibrium separation distance between the two atoms for the given separation distance R between the centers of masses of the two fragments.

The Cartesian components of the space-fixed rotational angular momentum for fragment i, j_{x_i} , j_{y_i} , and j_{z_i} are now given by

$$j_{x_i} = -p_{\phi_i} \cos \phi_i \cos \theta_i / \sin \theta_i - p_{\theta_i} \sin \phi_i$$

$$j_{y_i} = -p_{\phi_i} \sin \phi_i \cos \theta_i / \sin \theta_i + p_{\theta_i} \cos \phi_i$$

$$j_{z_i} = p_{\phi_i}$$
(18)

The inverse rotation matrix $\mathbf{A}_i^{-1}(\Omega_i)$ used to determine the transformation from orientational coordinates to space-fixed coordinates is given by⁷

$$\mathbf{A}_{i}^{-1}(\mathbf{\Omega}_{i}) = \begin{pmatrix} \cos \theta_{i} \cos \phi_{i} & -\sin \phi_{i} & \sin \theta_{i} \cos \phi_{i} \\ \cos \theta_{i} \sin \phi_{i} & \cos \phi_{i} & \sin \theta_{i} \sin \phi_{i} \\ -\sin \theta_{i} & 0 & \cos \theta_{i} \end{pmatrix}$$
(19)

The initial body-fixed coordinates $\mathbf{r}_{i,j}$ of atom j in fragment i must be aligned in agreement with the definition of the Cartesian components of the angular momenta given in eq 18. For this reason the axis of the linear fragment for these initial coordinates $\mathbf{r}_{i,j}$ is aligned along the space-fixed z axis, and the center of mass

$$\begin{array}{lll}
-\cos \psi_i \sin \phi_i - \cos \theta_i \cos \phi_i \sin \psi_i & \sin \theta_i \cos \phi_i \\
\cos \psi_i \cos \phi_i - \cos \theta_i \sin \phi_i \sin \psi_i & \sin \theta_i \sin \phi_i \\
\sin \psi_i \sin \theta_i & \cos \theta_i
\end{array} \tag{25}$$

of $\mathbf{r}_{i,j}'$ is placed at the origin. For the specific case of a diatomic fragment the body-fixed coordinates $\mathbf{r}_{i,j}'$ are thus given as

$$\mathbf{r}_{i,1}' = \left(0, 0, \frac{m_2}{m_1 + m_2} r_{\mathbf{e}}(R)\right)$$

$$\mathbf{r}_{i,2}' = \left(0, 0, \frac{-m_1}{m_1 + m_2} r_{\mathbf{e}}(R)\right) \tag{20}$$

The free-rotation canonical partition function for use in the averaging in eq 12 is¹¹

$$Q_i^0 = \frac{1}{h^2} \int \exp(-\beta T_i^0) \sin \theta_i \, d\Omega_i \, d\mathbf{p}_i'$$

$$= 2I_i^{\dagger} k_{\rm B} T / \hbar^2$$
(21)

where no degeneracy factor need be included in a partition function used purely for averaging.

(d) Nonlinear Fragment. When fragment i is nonlinear, the treatment is analogous to that given previously in part 1, where the dissociation into two nonlinear fragments was treated. The results are given here for completeness. The orientational coordinates are taken to be the Euler angles θ_i , ϕ_i , and ψ_i . Their conjugate momenta are then denoted by p_{θ_i} , p_{ϕ_i} , and p_{ψ_i} respectively. The transformed momenta are given by $\mathbf{p}_i' = (p_{a_i}, p_{b_i}, p_{c_i})$ with⁸

$$p_{a_i} = -\cos \psi_i \csc \theta_i p_{\phi_i} + \cos \psi_i \cot \theta_i p_{\psi_i} + \sin \psi_i p_{\theta_i}$$

$$p_{b_i} = \sin \psi_i \csc \theta_i p_{\phi_i} - \sin \psi_i \cot \theta_i p_{\psi_i} + \cos \psi_i p_{\theta_i}$$

$$p_{c_i} = p_{\psi_i}$$
(22)

The Jacobian $|\partial \mathbf{p}_i/\partial \mathbf{p}_i'|$ is then equal to $\sin \theta_i$.

For the kinetic energy of fragment i the specific expression depends on whether the fragment is an asymmetric top, a symmetric top, or a spherical top. Since all cases are included in the asymmetric top expression, we employ it. In terms of the transformed momenta \mathbf{p}_i' this kinetic energy is given by⁸

$$T_i^0 = \frac{p_{a_i}^2}{2I_{A_i^{\dagger}}} + \frac{p_{b_i}^2}{2I_{B_i^{\dagger}}} + \frac{p_{c_i}^2}{2I_{C_i^{\dagger}}}$$
 (23)

where $I_{A_i}^{\dagger}$, $I_{B_i}^{\dagger}$, and $I_{C_i}^{\dagger}$ are the principal moments of inertia of fragment *i* for the transition-state structure.

The Cartesian components of the space-fixed rotational angular momentum for fragment i, j_{x_l} , j_{y_l} , and j_{z_l} are given in terms of the transformed momenta \mathbf{p}_i' by

$$j_{x_i} = (\cos \theta_i \cos \phi_i \cos \psi_i - \sin \phi_i \sin \psi_i) p_{a_i} - (\cos \theta_i \cos \phi_i \sin \psi_i + \sin \phi_i \cos \psi_i) p_{b_i} + \sin \theta_i \cos \phi_i p_{c_i}$$

$$j_{y_i} = (\cos \theta_i \sin \phi_i \cos \psi_i + \cos \phi_i \sin \psi_i) p_{a_i} + (\cos \phi_i \cos \psi_i - \cos \theta_i \sin \phi_i \sin \psi_i) p_{b_i} + \sin \theta_i \sin \phi_i p_{c_i}$$

$$j_{z_i} = -\sin \theta_i \cos \psi_i p_{a_i} + \sin \theta_i \sin \psi_i p_{b_i} + \cos \theta_i p_{c_i} \quad (24)$$

The inverse rotation matrix $\mathbf{A}_i^{-1}(\Omega_i)$ used to determine the transformation from orientational coordinates to space-fixed coordinates is given by eq 25 of Chart I.⁷ The initial body-fixed coordinates \mathbf{r}_{ij} must be aligned in agreement with the definition of the Cartesian components of the angular momenta given in eq 24. Thus, the principal axes a, b, and c for these body-fixed coordinates \mathbf{r}_{ij} are aligned along the space-fixed x, y, and z axes, respectively. Additionally, the center of mass of \mathbf{r}_{ij} is at the origin.

⁽¹¹⁾ McQuarrie, D. A. Statistical Mechanics; Harper and Row: New York 1976

The definition of the free-rotation canonical partition function for use in the averaging is11

$$Q_i^0 = \frac{1}{h^3} \int \exp(-\beta T_i^0) \sin \theta_i \, d\Omega_i \, d\mathbf{p}_i'$$
$$= (8\pi I_i^A {}^{\dagger} I_i^B {}^{\dagger} I_i^C {}^{\dagger})^{1/2} (k_B T)^{3/2} / \hbar^3$$
(26)

IV. Trend of R^{\dagger} with Increasing Energy E

In several calculations^{3,5,10,12,13} we and others have noticed a tendency of R^{\dagger} , the fragment-fragment separation distance in the transition state, to decrease with increasing energy E. This effect has certain important consequences, which we describe after first considering its origin analytically.

The position R^{\dagger} of the transition state is the solution of

$$\partial N_{EI}(R^{\dagger})/\partial R^{\dagger} = 0 \tag{27}$$

which yields, implicitly, R^{\dagger} as a function of E. We may write the left-hand side as a function $f(R^{\dagger},E)$ and note that in the standard way the ordinary derivative dR^{\dagger}/dE is given by

$$dR^{\dagger}/dE = -(\partial f/\partial E)/(\partial f/\partial R^{\dagger}) \tag{28}$$

But $\partial f/\partial R^{\dagger}$ equals $\partial^2 N_{EJ}(R^{\dagger})/\partial R^{\dagger^2}$, and this quantity is positive since $N_{EJ}(R)$ is a minimum at $R=R^{\dagger}$. Further, upon interchanging the order of partial differentiation, $\partial f/\partial E$ can be written as $(\partial/\partial R^{\dagger})(\partial N_{EJ}(R^{\dagger})/\partial E)$, i.e., $(\partial/\partial R^{\dagger})\rho_{EJ}^{\dagger}(R^{\dagger})$, where $\rho_{EJ}^{\dagger}(R^{\dagger})$ is the density of states, $\partial N_{EJ}(R)/\partial R$, of the transition state at R $= R^{\dagger}$ and at the energy E. It has usually been the case that since the hindered rotations at smaller R become free rotations at larger R and, hence, that the states become more closely spaced as R increases, $(\partial/\partial R^{\dagger})\rho_{EJ}^{}(R^{\dagger})$ tends to be positive. One circumstance could modify this. As R increases, there will be somewhat less energy available for distribution among the transitional modes. since the bonding potential energy of the fragments is less negative. This factor above would make $\partial \rho_{EJ}^{\dagger}(R^{\dagger})/\partial R^{\dagger}$ negative, but apparently the first factor is the dominant one in the few cases we have considered thus far and for the limited energy range for which the model potential energy surfaces used are valid. At higher energies (e.g., above about 3000 cm⁻¹ for the study of ref 10) the model potential energy surfaces are not accurate enough and so no conclusions may be drawn as to which of the above factors is the dominant one.

This result on dR^{\dagger}/dE has some major implications: At very low energies E the R^{\dagger} occurs at the $R \rightarrow \infty$ limit and phase space theory⁶ (PST) and the variationally implemented RRKM theory become rather similar. However, with increasing energy the overall minimum in the number of states $N_{EJ}(R^{\dagger})$ occurs at R's which are less than the PST R_l 's, where the latter denote the location of the orbital angular momentum (1)-dependent effective potential energy barriers. As a result, at these energies, when dR^{\dagger}/dE is negative, there is increasing deviation between PST and variationally implemented RRKM theory; i.e., the transition state under these conditions becomes increasingly "tight". Again, in the case of fragment-fragment recombination this effect, when thermally averaged to yield a high-pressure rate constant, yields an R^{\dagger} which decreases as the temperature increases. Such an effect causes the high-pressure recombination rate constant to decrease with increasing temperature. 3,4,12,13

V. Case of Two Minima in the $N_{EJ}(R)$ Plot

From our previous calculations we have found that in a certain energy range there may be two local minima in the number of states. In particular, we have observed the following change in the plot of the number of states versus R as the energy E is increased above the dissociation limit: At low excess energies there is basically only one minimum (or smallest value) which occurs at $R^{\dagger} = \infty$. At slightly higher excess energies an inner minimum appears with this inner minimum being very shallow and having a much larger number of states than the $R^{\dagger} = \infty$ one. At still higher energies the number of states at the inner minimum begins to approach the number at the $R^{\dagger} = \infty$ minimum. Our potential energy surface needs improvement at smaller R^{\dagger} 's to see how the trend changes as E is increased further.

In the energy region where there are two transition states it is useful to consider the modified formalism resulting from the two transition states which act in series. In the case of the recently studied NCNO dissociation reaction, 10 $N_{EJ}^{\rm max}$ typically proved to be a small maximum relative to the larger value of the number of states occurring at each of the two minima, i.e., $N_{EI}^{\text{max}} \approx$ max (N_{EJ}^1, N_{EJ}^2) , where N_{EJ}^1 and N_{EJ}^2 are the number of states for the two minima. Thus, the various two-transition state theories 14,15 largely reduced almost everywhere to eq 1, where $N_{EJ}(R^{\dagger})$ now denotes the smaller of N_{EJ}^1 and N_{EJ}^2 . In particular, we found that the rate constants calculated from the lower bound formula given below differed by at most a factor of 0.5 from those calculated with eq 1, using in the latter the global minimum for $N_{EJ}(R^{\dagger})$. Additionally, the rate constant obtained from the "unified statistical theory" discussed below differed by at most a factor of

A treatment of the typical situation in chemical reactions when there are two values of R where the reactive flux may be reflected and/or transmitted was first given by Hirschfelder and Wigner. 16 Subsequently, Miller¹⁴ introduced into that formalism expressions for the reflection probabilities in terms of statistical flux ratios (or equivalently in terms of the number of states) and obtained a "unified statistical theory" (UST). As noted by Chesnavich et al., 17 when these ideas are applied to a unimolecular dissociation reaction the rate constant is given by¹⁷

$$k_{EJ} = \frac{1}{h\rho_{EJ}} \frac{N_{EJ}^{\dagger 1} N_{EJ}^{\dagger 2}}{N_{EJ}^{\dagger 1} + N_{EJ}^{\dagger 2} - N_{EJ}^{\dagger 1} N_{EJ}^{\dagger 2} / N_{EJ}^{\max}}$$
(29)

Subsequently, studies by Pollak et al. 15 showed that the assumption embodied in eq 29 of having statistically determined reflection probabilities is not a good one at all energies. For simple reactions such as $H + H_2 \rightarrow H_2 + H$ and $F + H_2 \rightarrow FH + H$, UST was shown to give substantially larger reaction probabilities at high energies than those determined from classical trajectories. Pollak et al. 15 then presented a method for determining a lower bound for the reaction probabilities based on consideration of only those trajectories which cross the maximum flux surface 2 times or less. The dynamical results of ref 15 were shown to be in significantly better agreement with the lower bound probabilities than with UST for the cases examined. This result can once again be directly applied to the unimolecular dissociation case, and the rate constant is then given by

$$k_{EJ} = \frac{(N_{EJ}^{\uparrow 1} + N_{EJ}^{\uparrow 2} - N_{EJ}^{\text{max}})}{h\rho_{EJ}}$$
 (30)

However, as already noted, for the NCNO system we have studied, formulas 29 and 30 reduce in practice to eq 1, with N_{EJ}^{\dagger} having now the smaller of the number of states at the two local minima.

VI. Role of the Repulsive Curves in Unimolecular

Typically, in a unimolecular dissociation into two fragments there are two or more potential energy curves, for example the singlet and triplet curves in Figure 1. If phase space theory is applied, 18 the *l*-dependent effective potential energy barriers may occur at such large separation distances that these curves are almost degenerate at the barrier maximum, and the question arises

⁽¹²⁾ Rai, S. N.; Truhlar, D. G. J. Chem. Phys. 1983, 79, 6046.

⁽¹³⁾ Hase, W. L. Chem. Phys. Lett. 1987, 139, 389, and references cited therein. Quack, M.; Troe, J. Ber. Bunsen-Ges Phys. Chem. 1977, 81, 329. Smith, G. P.; Golden, D. M. Int. J. Chem. Kinet. 1978, 10, 489. Benson, S. W. Can. J. Chem. 1983, 61, 881.

⁽¹⁴⁾ Miller, W. H. J. Chem. Phys. 1976, 65, 2216.

⁽¹⁵⁾ Pollak, E.; Pechukas, P. J. Chem. Phys. 1979, 70, 325. Pollak, E.;

Child, M. S.; Pechukas, P. J. Chem. Phys. 1980, 72, 1669.
(16) Hirschfelder, J. O.; Wigner, E. J. Chem. Phys. 1939, 7, 616.
(17) Chesnavich, W. J.; Bass, L.; Su, T.; Bowers, M. T. J. Chem. Phys. 1981, 74, 2228. Calcultions using the unified statistical model are also described in ref 12.

⁽¹⁸⁾ For other discussions of which states to include in PST calculations see, for example: Herbst, E.; Knudson, S. K. Chem. Phys. 1981, 55, 293.

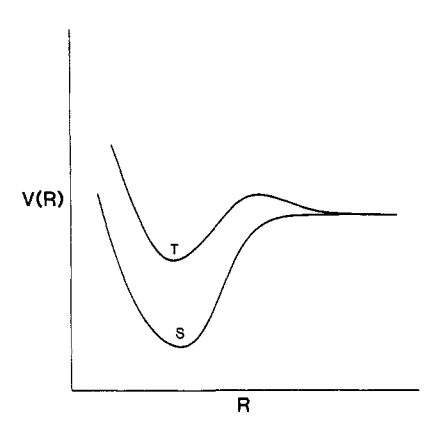


Figure 1. Schematic diagram of potential energy curves for typical unimolecular dissociation into two fragments. S denotes the lower singlet level, and T denotes the upper triplet level. V(R) is the minimum potential energy for a given center-of-mass to center-of-mass separation distance R.

whether both the singlet and triplet levels or just the singlet one should be used in the PST calculation. In the variational RRKM method, on the other hand, the R^{\dagger} moves to shorter fragment-fragment separation distances, even when the excess energy is quite small (e.g., when $E \approx 500~\rm cm^{-1}$ in both the $C_2H_6 \rightarrow 2CH_3$ and the NCNO \rightarrow NC + NO cases). In particular, it moves to a value where the singlet-triplet splitting becomes fairly large relative to the excess energy. In this case the contribution of the triplet state to N_{EJ}^{\dagger} becomes relatively minor. Moreover, it is also arguable whether there would be time between R^{\dagger} and the PST R_I for the system to undergo an intersystem crossing from the singlet to the triplet state.

Thus, in our past and current applications we have largely confined our attention to calculating N_{EJ}^{\dagger} from the singlet curve, rather than from any excited-state curves. We have examined in detail in ref 10 the case of NCNO decomposition. Here, there is the ground-state singlet S_0 and a weakly bound triplet T_1 , both leading to the quadruply degenerate asymptotic state $(NO_{1/2},CN)$. There are also the upper repulsive singlet S_1 and T_2 curves, leading to an asymptote $(NO_{3/2},CN)$ 120 cm⁻¹ higher in energy than that of $(NO_{1/2},CN)$. The upper two curves (ref 10) may be disregarded in the reaction rate calculation, for the reason described in the previous paragraph. We found, using an approximate potential energy function and assuming rapid singlet—triplet conversions, that the lower triplet T_1 state made a contribution to N_{EJ}^{\dagger} only at low E's. But even the inclusion of that contribution becomes uncertain if the singlet—triplet conversion rate is not high in the transition-state region.

VII. Concluding Remarks

General formulas for determining $N_{EJ}(R)$, the number of states as a function of center-of-mass to center-of-mass separation for the various possible fragment cases, have been presented. From the specific formulas given for the three different possible types of fragments the overall computational expression for any combination of two fragments is immediately obtained. In particular, eq 12 and 13 are used with the combinations (sum, product, etc.) of the formulas given for the two separate types of fragments. This method is a general one and may be easily applied to a large variety of unimolecular dissociation reactions. The method can also be modified to treat unimolecular isomerizations, in which case there is only one fragment. It has been applied in recent papers to experimental data on the unimolecular dissociation reactions $C_2H_6 \rightarrow 2CH_3^5$ and $NCNO \rightarrow NC + NO.^{10}$

In the application of this method the uncertain quantity is the molecular potential energy surface. In previous applications^{3,5,10} model potential energy surfaces were used. At short separation distances the repulsive interactions between the nonbonded atoms are much too strong in these model potential energy functions. We found as a result that there appeared to be no local minimum in the $N_{EJ}(R)$ plot at energies above about 3000 cm⁻¹ for the $NCNO \rightarrow NC + NO$ reaction. This disappearance of the local minimum in $N_{EJ}(R)$ indicates the need for more accurate potential energy surfaces. A further indication of just how strongly repulsive the model potential energy surface is at short distances is given by the comparison of $N_{E,I}(R)$ at $R = R_e$ with the number of states for the reactant (excluding the dissociation coordinate) as determined by Whitten-Rabinovitch type calculations. These two quantities are given by 0.1×10^7 and 4×10^7 , respectively, for an excess energy of 2348 cm⁻¹ and a total angular momentum of 5, for the parameters in ref 10. One hope is that studies such as those of ref 10 will motivate the ab initio calculation of potential energy surfaces for the fragment-fragment hindered rotational motions at center-of-mass to center-of-mass separation distances near R^{\dagger} (about 3.0-4.5 Å for the NCNO \rightarrow NC + NO reaction).

We have also presented here arguments providing some insight into the previously observed trend of R^{\dagger} decreasing with increasing energy. This trend indicates a larger deviation with increasing energy of RRKM rates from those of PST. A discussion of the various formulas for considering the effect of two transition states in series has also been given, along with a consideration of their importance in unimolecular dissociation reactions. Finally, a discussion of which potential energy surfaces should be used in unimolecular dissociation rate calculations has also been given.

Acknowledgment. We are pleased to acknowledge the support of this research by a grant from the National Science Foundation.

High-Resolution Fluorescence Excitation Spectroscopy of S₁ Formaldehyde-d₂

Joan K. Frisoli, William F. Polik, and C. Bradley Moore*

Department of Chemistry, University of California, Berkeley, California 94720 (Received: February 2, 1988)

Rotationally resolved fluorescence excitation spectra are measured and assigned for vibrational bands 4^2 , 2^14^1 , 1^14^1 , 5^1 , $2^14^26^1$, 2^24^3 , 2^15^1 , and $2^14^25^1$ in the \tilde{A}^1A_2 state of D_2CO in a cold supersonic molecular beam. The rotational constants and origins of each vibrational band are obtained. Several new vibrational bands are observed, and approximate band centers measured with 1-cm⁻¹ resolution.

Introduction

The history of formaldehyde spectroscopy, photophysics, and photochemistry is both long and interesting, ^{1,2} and much of it has unfolded in the laboratories of E. K. C. Lee.³ Studies on the forefront of chemical physics continue to focus on formaldehyde

because it is large enough to undergo complex photochemistry⁴ and small enough to be theoretically tractable.⁵ High-resolution

[†]Present address: Wellman Laboratory, Massachusetts General Hospital, Boston, MA 02114.

Moore, C. B.; Weisshaar, J. C. Ann. Rev. Phys. Chem. 1983, 34, 525.
 Clouthier, D. J.; Ramsay, D. A. Ann. Rev. Phys. Chem. 1983, 34, 31, and references therein.

⁽³⁾ Sodeau, J. R.; Lee, E. K. C. Rev. Chem. Intermed. 1980, 4, 259, and references therein

⁽⁴⁾ Chuang, M.-C.; Foltz, M. F.; Moore, C. B. J. Chem. Phys. 1987, 87, 8855